Supplementary Material

Insights into the Nitrogen-vacancy Center Formation in Type-Ib Diamond by Irradiation and Annealing Approach

Taiqiao Liu[1,†], Fanglin Lyu[2,†], Tian Shao[2], Diwei Zou[1], Wei Shen[1,*], Yuzheng Guo[3], Yuan Zhong[2], Chaoyang Chen[2], Liangchen Yi[4], Zhaofu Zhang[1,5,*] and Andy H. Shen[2,*]

[1] The Institute of Technological Sciences, Wuhan University, Wuhan, 430072, China

[2] Gemmological Institute, China University of Geosciences, Wuhan, 430074, China

[3] School of Electrical Engineering and Automation, Wuhan University, Wuhan 430072, China

[4] Zhongnan Diamond Company, Nanyang, 473264, China

[5] Hubei Key Laboratory of Electronic Manufacturing and Packaging Integration, Wuhan University, Wuhan 430072, China

† These authors contributed equally to this work.

∗ Authors to whom any correspondence should be addressed. E-mail address: zhaofuzhang@whu.edu.cn (Zhaofu Zhang); wei_shen_@whu.edu.cn (Wei Shen); shenxt@cug.edu.cn (Andy H. Shen)

The expressions of potential functions are as follows:

$$E = \frac{1}{2}\sum_i \sum_{j\neq i} V_{ij} \quad \text{(Eq. 1)}$$

$$V_{ij} = \left(1 - f_F(r_{ij})\right) V^{ZBL}(r_{ij}) + f_F(r_{ij}) V^{Tersoff}(r_{ij}) \quad \text{(Eq. 2)}$$

$$f_F(r) = \frac{1}{1+e^{-A_F(r-rC)}}$$

$$f_C(r_{ij}) = \begin{cases} 1, & r_{ij} < R_{ij} \\ \frac{1}{2} + \frac{1}{2}\cos\left(\pi \frac{r_{ij}-R_{ij}}{S_{ij}-R_{ij}}\right), & R_{ij} < r_{ij} < S_{ij} \\ 0, & r_{ij} > R_{ij} \end{cases}$$

$$f_C(r_{ik}) = \begin{cases} 1, & r_{ik} < R_{ik} \\ \frac{1}{2} + \frac{1}{2}\cos\left(\pi \frac{r_{ik}-R_{ik}}{S_{ik}-R_{ik}}\right), & R_{ik} < r_{ik} < S_{ik} \\ 0, & r_{ik} > R_{ik} \end{cases}$$

$$f_R(r_{ij}) = A_{ij}\exp(-\lambda_{ij}^{I} r_{ij}),\ f_A(r_{ij}) = -B'_{ij}\exp(-\lambda_{ij}^{II} r_{ij}),$$

$$B'_{ij} = B_{ij}\chi_{ij},\ b_{ij} = (1 + \beta_i^{n_i}\zeta_{ij}^{n_i})^{-\frac{1}{2n_i}},$$

$$\zeta_{ij} = \sum_{k\neq i,j} f_C(r_{ik})\, g(\theta_{ijk}),$$

$$g(\theta_{ijk}) = 1 + \frac{c_i^2}{d_i^2} - \frac{c_i^2}{[d_i^2 + (\cos\theta_{ijk} - h_i)^2]}.$$

$$V^{ZBL}(r_{ij}) = \frac{1}{4\pi\epsilon_0}\frac{Z_1 Z_2 e^2}{r_{ij}}\phi(x), \quad \text{(Eq. 3)}$$

$$x = \frac{r_{ij}\left(z_1^{0.23}+z_2^{0.23}\right)}{a_0},$$

$$\phi(x) = 0.1812e^{-3.2x} + 0.5099e^{-0.9423x} + 0.2802e^{-0.4029x} + 0.02817e^{-0.2016x}$$

where the f_F is a Fermi-like function used to smoothly connect the Tersoff and ZBL potential functions, which is mainly regulated by two parameters, A_F and r_C. A_F controls how "sharp" the transition is between the two, and r_C is essentially the cutoff for the ZBL potential. The subscripts i, j, k denote atoms and r_{ij} is the distance between atoms i and j. For the Tersoff potential, f_R is the repulsive potential function, f_A is the attractive potential function, and f_C is a smooth cutoff function that limits the range of the potential on the nearest-neighbor atom interaction. g (θ_{ijk}) is the bond angle between the i-j and i-k pairs.

For the ZBL potential, Z_1 and Z_2 denote the number of protons in each nucleusi and j. a_0 is the Bohr radius (typically 0.05292 nm). ϵ_0 is permittivity of vacuum that equals. And e is the electron charge.

Table S1. The interaction potentials of Tersoff and ZBL for the diamond NV system. Note that the r_C and A_F for N-C and N-N interactions were originally derived in this work.

Elements	C-C	N-C	N-N
A(eV)	1.5448e3	1.1000e4	128.8687
B'(eV)	3.8963e2	2.1945e2	138.7787
λ^I(Å^{-1})	3.4653	5.7708	5.9798
λ^{II}(Å^{-1})	2.3064	2.5115	5.5436
B (10^{-7})	4.1612e-6	1.0526e-1	1.9278
N	9.9054e-1	12.4498	0.665
C	1.9981e4	7.9934e4	23.5
D	7.034e0	1.3432e2	3.75
H	-3.3953e-1	-0.9973	-0.4
R(Å)	1.95	2.0	1.8
S(Å)	2.10	2.3	2.0
A_F(Å^{-1})	14	25 (this work)	20 (this work)
r_c(Å)	0.33	0.05 (this work)	0.9 (this work)

Molecular dynamics simulation calculation details

The simulation systems were first equilibrated for 20 ps within the canonical ensemble (NVT), with a time step of 1 fs. Subsequently, irradiation was applied for 50 ps under variable time steps within the microcanonical ensemble (NVE). The time step was reset to a lower value if its displacement exceeded 0.005 a_0 in a single molecular dynamics (MD) time step. The maximum allowed time step was 0.5 fs. The isothermal-isobaric ensemble (NPT) with a time step of 0.5 fs was adopted for the annealing procedure. The heating and cooling rates were maintained at 1 K/ps with a holding time of 500 ps, resulting in a total annealing duration of 2100 ps. The temperature variation over time during the entire process is depicted in Fig. S2. A total of 48 simulations were conducted for the diamond model containing randomly doped 900 ppm nitrogen. The number of repetitions under each condition is shown in Table S1. Since given experimental findings indicating that NV centers are most easily generated at 1073 K [1-4], simulations were conducted six times in each direction at this temperature and five times at all other temperatures.

Table S1. The frequency of repetitions under various conditions in MD simulation. A total of 48 repetitions was conducted in this work.

Simulation time	2100 ps		
Annealing temperature / Orientation	973 K	1073 K	1173 K
[111]	5	6	5
[110]	5	6	5
[100]	5	6	5

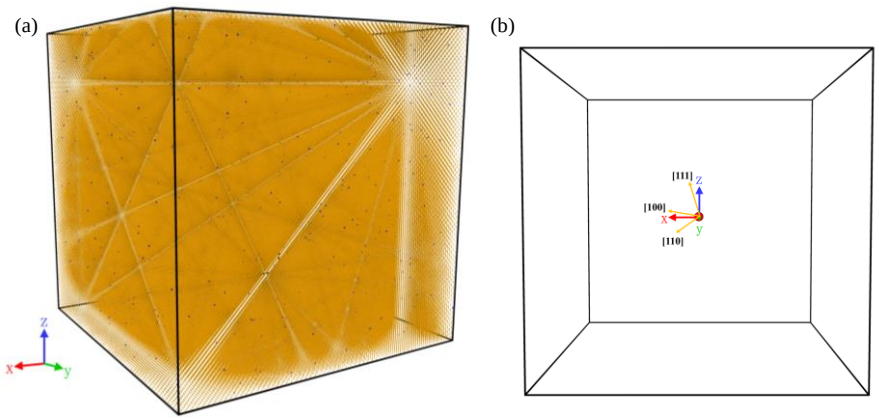

Fig. S1. (a) Nitrogen-doped diamond model diagram with one million atoms. The yellow dots represent carbon atoms, while the blue dots represent nitrogen atoms. (b) Schematic diagram of the incident direction of PKA. The PKA is represented by the red atom in the box's center.

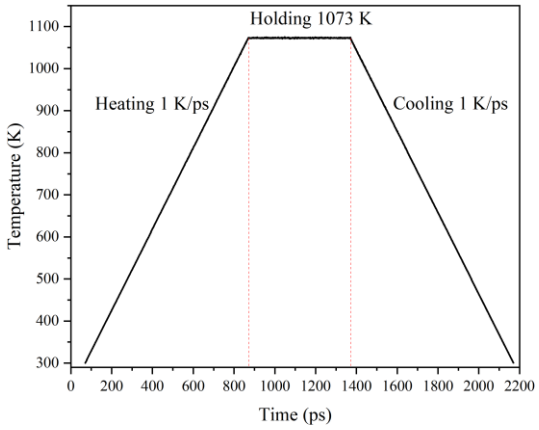

Fig. S2. The derived temperature variation versus the time. The holding temperature at 1073 K is adopted in this case.

According to the absorption peak intensity of nitrogen impurities in the measured in-situ Fourier Transform Infrared Spectrometer (FTIR) spectra, the nitrogen concentration in the sample can be quantitatively calculated. Previous research indicates that the concentration of neutral isolated nitrogen N_s^0 is proportional to the absorption intensity of the characteristic absorption peaks at 1130 cm^{-1} and 1344 cm^{-1} in the infrared spectrum. The absorption coefficient of the 1130 cm^{-1} peak was primarily used to calculate the concentration of the nitrogen centers in this experiment. The calculation formula is as follows [5-11]:

$$N_s^0 = (25.0 \pm 2)\ \mu_{1130} \quad \text{(Eq. 4)}$$

where N_s^0 is the concentration of N_s^0, measured in ppm. μ_{1130} is absorption coefficient,

measured in cm^{-1}. Therefore, the maximum consentration of N_s^0 is estimated by the spectral peak 1130 cm^{-1} to be 18.5 ppm atom.

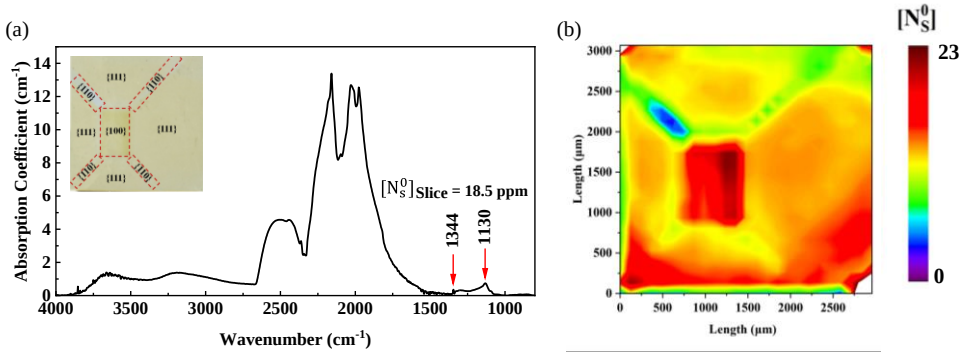

Fig. S3. The *in-situ* Fourier Transform Infrared Spectrometer (FTIR) spectra of the diamond slice before irradiation. (a) The typical spectra showing absorption peaks at 1344 cm^{-1} and 1130 cm^{-1} both from neutral isolated nitrogen (N_s^0), based on the latter the maximum consentration of N_s^0 ($[N_s^0]$) is estimated to be 18.5 ppm atom. (b) The distribution of $[N_s^0]$ across the slice (also estimated from the mapping of 1130 cm^{-1} peak). FTIR spectra were collected by a Bruker v80 + Hyperion 3000 micro IR spectrometer, and strong spatial correlation can be recognized between the color pattern and the distribution of N_s^0.

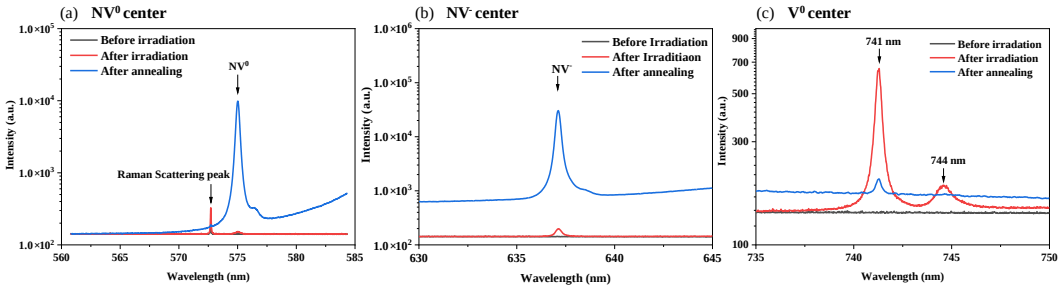

Fig. S4. The PL peaks of (a) NV^0, (b) NV^- and (c) V^0 signals before irradiation, after irradiation and after annealing. V^0 will split into two peaks of 741 nm and 744 nm at low temperature (~77 K). In Fig. 6, the PL peak mapping of V^0 is obtained by 741nm.

Fig. S5(a) shows the number of Frenkel pairs of type-Ib diamond as a function of time along three directions. Thermal spikes are reported to be absent in diamonds [14]. However, in our work, thermal spikes are absent in [111] and [100], but remain in [110]. Fig. S5(b)-(d) shows three-dimensional snapshots of point defects after irradiation, where yellow, blue and red spheres represent vacancies, interstitial and PKA atoms in a cascade collision along the blue trajectory lines, respectively. From these snapshots, it is concluded that 1) the vacancies are distributed along the trajectory lines, which is consistent with previous studies [14, 15] and demonstrates the suitability of the

potential candidates, and 2) the [110] direction has the fewest vacancies.

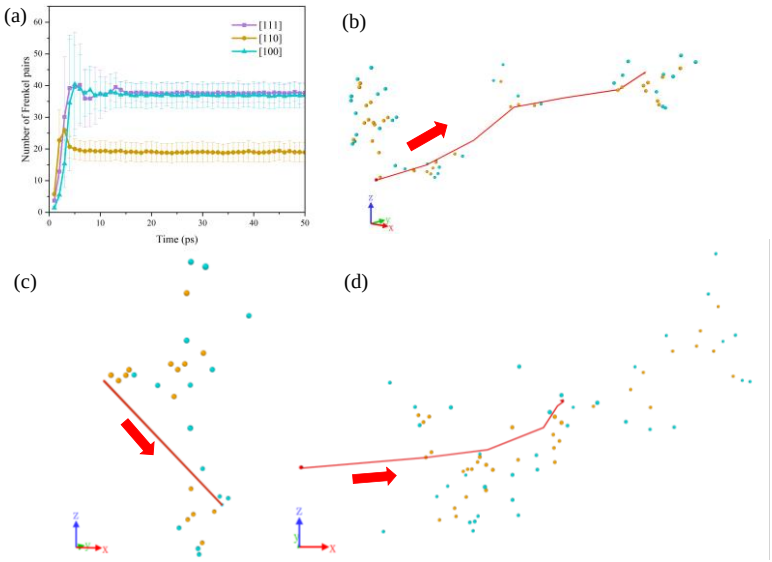

Fig. S5. The number of Frenkel pairs as a function of time (a) and the distribution of point defects along (b) [111] direction, (c) [110] direction, and (d) [100] direction, respectively. The yellow balls are vacancies, the blue balls are interstitial atoms, and the blue balls are PKA atoms colliding in cascade along the blue trajectory lines.

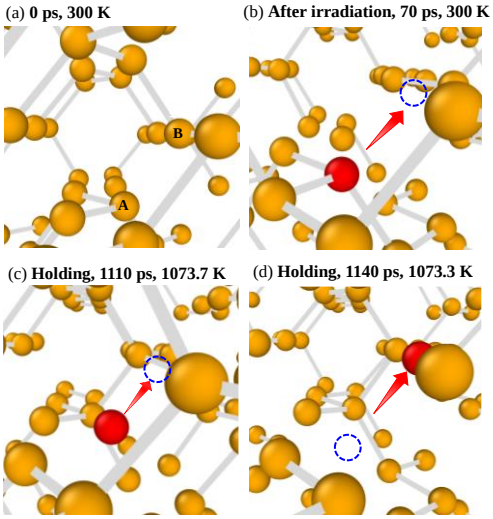

Fig. S6. (a-d) The MD snapshots of a single vacancy migration during the irradiation and annealing processes in diamond. The vacancy site is represented by a dashed blue circle. The red arrow represents one carbon atom (at the A-site) progressively moving to the B-site as the increased temperature during annealing. Notably, the vacancy undergoes a positional shift from the B-site to the A-site.

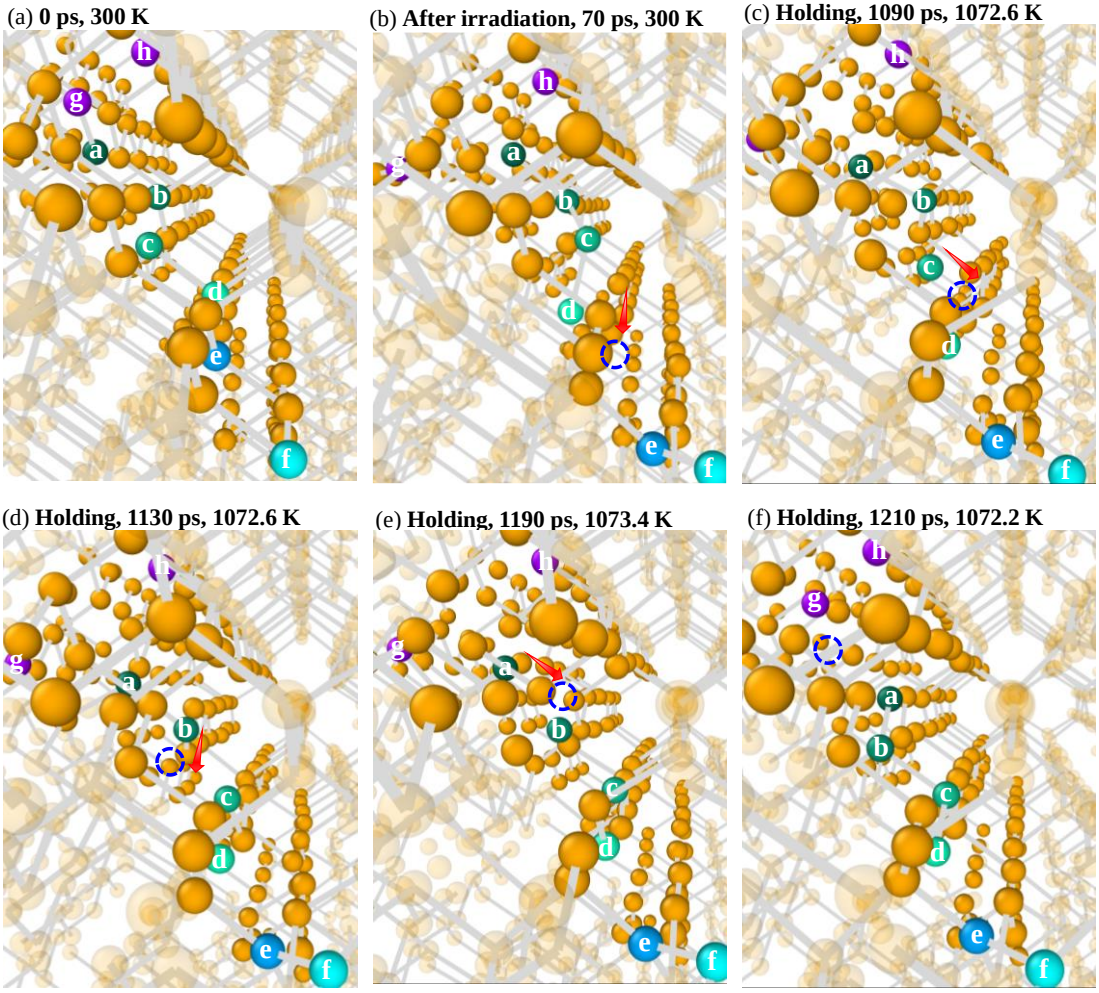

Fig. S7. The MD snapshots of a single vacancy migrating multiple times during the irradiation and annealing processes in diamond. The vacancy site is represented by a dashed blue circle. The red arrow represents one carbon atom (at the e-site) progressively moving to the a-site as the increased temperature during annealing. The vacancy migrates in the following directions from beginning to end: e→d, d→c, c→b, and b→a.

The snapshots depicted in Fig. S6 display the phenomenon of multiple vacancy migrations. The atoms labeled from a to h denote the sites where the migration process occurs. Before irradiation, all atoms are in their lattice sites (Fig. S7(a)). Subsequent to radiation exposure, the carbon atom in the e-site forms a split-interstitial with f-atom, resulting the e-site becoming a vacancy (Fig. S7(b)). Concurrently, carbon atoms in c, d, g, and h sites also exhibit deviations from their lattice sites. At 1090 ps and temperature of 1072.6 K (Fig. S7(c)), the vacancy migrates to the d-site. Continuing at the same temperature, the vacancy migrates to the c-site after 40 ps (Fig. S7(d)) and to the a-site after 20 ps. At this point, the g-atom, both the g-atom, previously an interstitial

atom, and the h-atom, previously displaced from their lattice position, revert to their original positions. Finally, the vacancy sequentially migrates from the e-site to the a-site through four migration events.

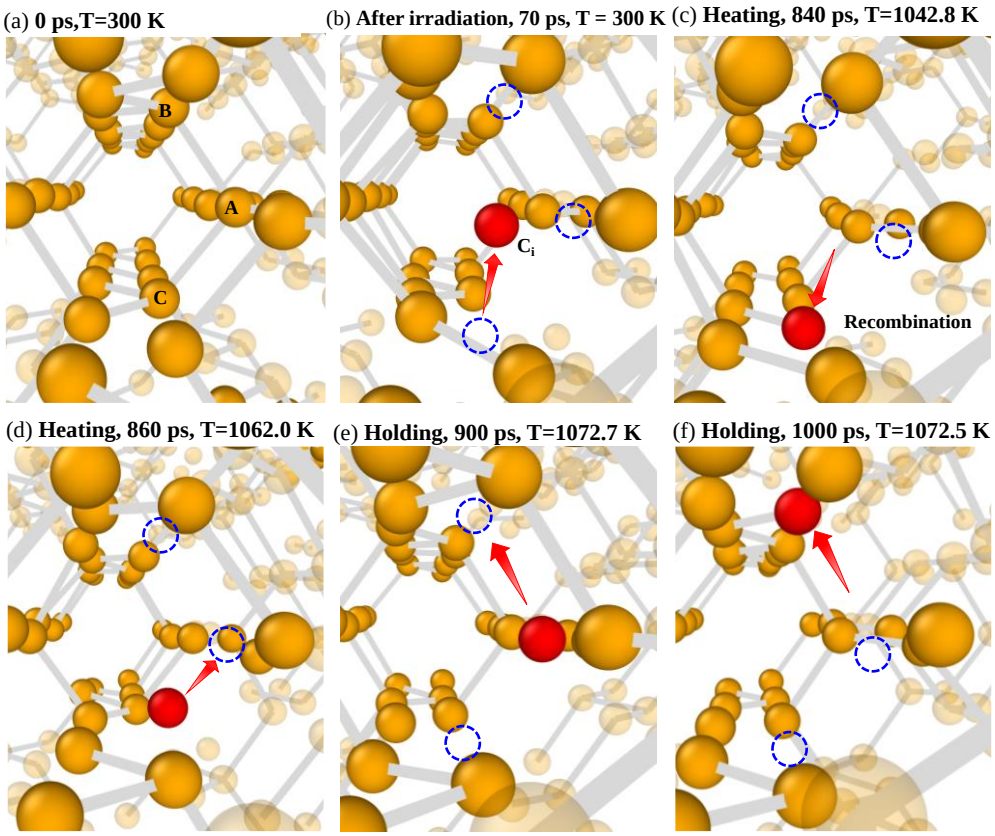

Fig. S8. (a-f) The MD snapshots of an exceptional case about vacancy migration. The dashed blue circles represent vacancies. The red arrows represent the migration paths. During the annealing process, the red interstitial atom Ci in (b) is drawn back to its initial vacancy site in (c), but eventually (d) moves to the A-vacancy site and (e) continues to move to the B-vacancy site with further annealing. Finally, the vacancy position shifts from (c) to (f).

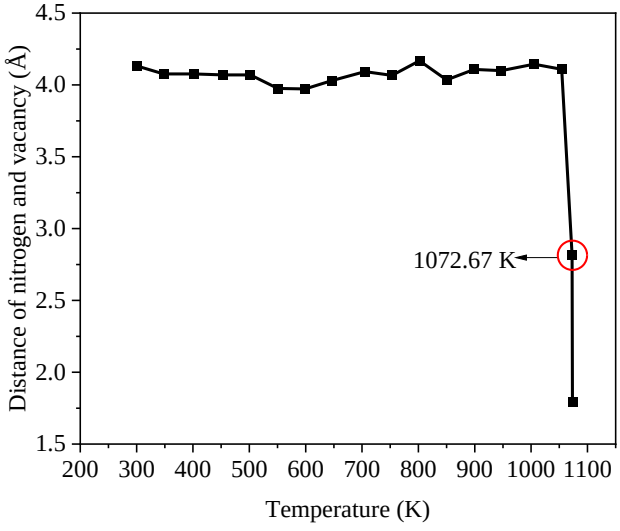

Fig. S9. The trend of the distance between nitrogen and vacancy with annealing temperature.

Crystal orientation dependence

Fig. S10(a) compares the minimum temperatures required for vacancy migration and NV center formation. It can be seen that the ability of vacancy migration follows the sequence [110] < [111] < [100], whereas the NV center formation ability adheres to the sequence [110] < [100] < [111], respectively, based on the minimum migration temperature. The ratio of NV center to the number of migrated-vacancy (#NV/#Migrated-vacancy) and the total number of vacancies (#NV/#total-vacancy) produced by irradiation is shown in Fig. 8(b). The #NV/#Migrated-vacancy for the [111], [110], and [100] directions are 10.52%, 2.5%, and 8.16%, respectively, while the corresponding #NV/#total-vacancy are 3.53%, 5.02%, and 4.38%. Thus, the propensity for vacancy migration to facilitate NV center formation exhibits a pronounced dependence on crystal orientation [110] < [100] < [111]. Notably, along the [110] direction, the least migrated vacancies are converted into NV centers. Simultaneously, a unique phenomenon was discovered where the highest number of NV centers were produced in the [110] direction, as indicated by the #NV/#Total-vacancy ratio. This phenomenon can be attributed to the relatively lower density of vacancies in this crystallographic orientation. NV center formation is related to the concentrations of vacancies and nitrogen [2, 3], suggesting that the minimum number of vacancies [11] and the highest minimum migrating temperature result in a predominantly irradiation-induced NV formation (INF) mechanism along [110] direction. The experimental results depicted in Fig. 6 of the manuscript demonstrate that after irradiation, NV^0 and NV^- centers are mainly localized in the {111} and {100} regions, respectively, with the highest V^0 signal observed in the {110} region. However, after annealing, V^0 signals are exclusively observable in the {110} growth region. This observation indicates that the formation of NV centers along the [110] direction presents challenging characteristics and is primarily formed through irradiation-induced processes.

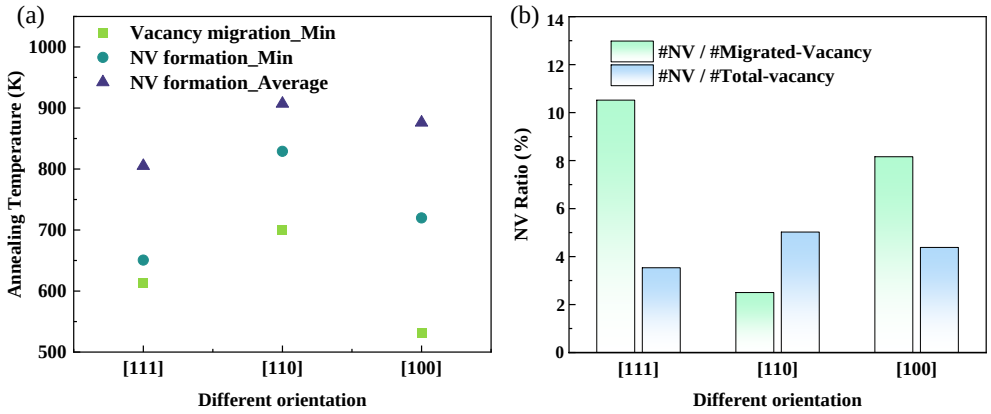

Fig. S10. The (a) annealing temperature and (b) vacancy migration and NV formation ratio in different diamond orientations. The # symbol represents the corresponding number.

Fig. S11 shows the average migrating time of vacancy at various annealing temperatures. The entire annealing time is 2100 ps. In [111] direction, the vacancy migrates the earliest at 973 K and the latest at 1073 K. 1073 K and 1173 K are only 10 ps apart. In the direction of [110], the vacancy migrates the earliest at 1073 K, with just a 5 ps difference between 973 K and 1173 K. In the direction of [100], the vacancy migrates the earliest at 1073 K, with a 31 ps difference between 973 K and 1173 K. The earlier the period of vacancy migration, the more probable the vacancy will migrate to form NV center with nitrogen. The results are consistent with the fact that the highest ratio of #NV / #migrated-vacancy in Fig. 8 of the manuscript in [111], [110] and [100] directions is at annealing temperature 973 K, 1073 K, and 1073 K, respectively.

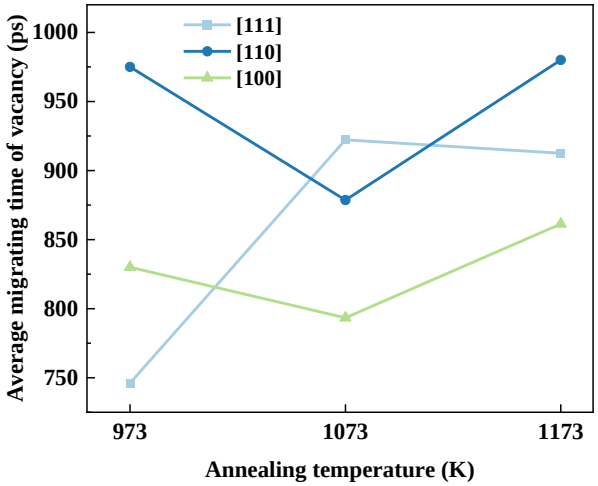

Fig. S11. The average migrating time of vacancy at different annealing temperature.

The animation videos for the mechanism of vacancy movement:

Supplementary_Video_1: Video for Fig. 3.

Supplementary_Video_2: Video for Fig. S7.

Supplementary_Video_3: Video for the special phenomenon in Fig. 4.

The animation videos for the mechanism of NV center formation:

Supplementary_Video_4: Video for the first mechanism (INF) in Fig. 5(a).

Supplementary_Video_5: Video for the second mechanism (IFA) in Fig. 5(b).

Supplementary_Video_6: Video for the third mechanism (VM) in Fig. 5(c).

References

[1] G.J. Davies, M.F. Hamer, Optical studies of the 1.945 eV vibronic band in diamond, Proceedings of the Royal Society of London. Series A 348 (1976) 285 - 298.
[2] A. Tallaire, O. Brinza, P. Huillery, T. Delord, C. Pellet-Mary, R. Staacke, et al., High NV density in a pink CVD diamond grown with N_2O addition, Carbon 170 (2020) 421-429.
[3] S. Kollarics, F. Simon, A. Bojtor, K. Koltai, G. Klujber, M. Szieberth, et al., Ultrahigh nitrogen-vacancy center concentration in diamond, Carbon 188 (2022) 393-400.
[4] J. Schwartz, S. Aloni, D.F. Ogletree, T. Schenkel, Effects of low-energy electron irradiation on formation of nitrogen-vacancy centers in single-crystal diamond, New Journal of Physics 14 (2012) 043024.
[5] S.C. Lawson, D. Fisher, D.C. Hunt, M.E. Newton, On the existence of positively charged single-substitutional nitrogen in diamond, Journal of Physics Condensed Matter 10 (1998) 6171-6180.
[6] I. Kiflawi, A. E. Mayer, P. M. Spear, J. A. Van Wyk, G. S. Woods. Infrared absorption by the single nitrogen and A defect centres in diamond, Philosophical Magazine B 69 (1994) 1141-1147.
[7] A. Collins, G. Woods. An anomaly in the infrared absorption spectrum of synthetic diamond, Philosophical Magazine B 46 (1982) 77-83.
[8] G. S. Woods, J. A. Van Wyk, & A. T. Collins, The nitrogen content of type Ib synthetic diamond, Philosophical Magazine B 62(1990) 589-595.
[9] G. Davies, Current problems in diamond: towards a quantitative understanding, Physica B: Condensed Matter 273 (1999) 15-23.
[10] Z.Z. Liang, J.Q. Liang, N. Zheng, X.P. Jia, G.J. Li. Optical absorbance of diamond doped with nitrogen and the nitrogen concentration analysis, Acta Physica Sinica 58 (2009) 8039.
[11] L. J. Su, C. Y. Fang, Y. T. Chang, K. M. Chen, Y. C. Yu, J. H. Hsu & H. C. Chang, Creation of high density ensembles of nitrogen-vacancy centers in nitrogen-rich type Ib nanodiamonds, Nanotechnology 24 (2013) 315702.
[12] C.X. Li, Q.Y. Zhang, N. Zhou, C. Zhang, Z. Yi. Impacts of nitrogen concentration and electron irradiation fluence on the formation of nitrogen-vacancy defects in diamond, Diamond and Related Materials 132 (2023) 109623.

[13] W. Wang, C. Fang, L. Chen, Z. Zhang, Y. Zhang, Q. Wang, et al., Effect of Fe_6N_2 on diamond growth under high pressure and high temperature conditions, Diamond and Related Materials, 142, (2024) 110863.
[14] J.T. Buchan, M. Robinson, H.J. Christie, D.L. Roach, D.K. Ross, N.A. Marks, Molecular dynamics simulation of radiation damage cascades in diamond, Journal of Applied Physics 117 (2015) 245901.
[15] T. Liu, T. Shao, F. Lyu, X. Lai, A.H. Shen, Molecular dynamics simulations to assess the radiation resistance of different crystal orientations of diamond under neutron irradiation, Modelling and Simulation in Materials Science and Engineering 30 (2022) 035005.